

A Study on the Edge Enhancement of X-ray Images Generated by a Gas Electron Multiplier Chamber

B. S. Moon, I. K. Hwang, C. E. Chung, K. C. Kwon
Korea Atomic Energy Research Institute
P.O. Box 105, Taeduk Science Town, Daejeon 305-600, Korea
E-mail:bsmoon@kaeri.re.kr
Fax:+82-42-868-8916

Abstract

In this paper, we describe the results of a study on the edge enhancement of X-ray images by using their fuzzy system representation. A set of gray scale X-ray images was generated using the EGS4 computer code. An aluminum plate or a lead plate with three parallel strips taken out has been used as the object with the thickness and the width of the plate, and the gap between the two strips varied. We started with a comparative study on a set of the fuzzy sets for their applicability as the input fuzzy sets for the fuzzy system representation of the gray scale images. Then we describe how the fuzzy system is used to sharpen the edges. Our algorithm is based on adding the magnitude of the gradient not to the pixel value of concern but rather to the nearest neighboring pixel in the direction of the gradient. We show that this algorithm is better in maintaining the spatial resolution of the original image after the edge enhancement.

Keywords: X-ray images; Spatial Resolution; Fuzzy Systems; Gradient Operator; Gray Scale Images; EGS4

1. INTRODUCTION

Edge enhancement [1] is a digital image processing filter that is used to make pictures artificially sharper than they really are. To make the pictures look sharper without more details being added, one must detect the boundaries where the image intensity changes sharply and increase the intensities at the pixels with higher intensities while suppressing the pixels of the lower intensities. The most commonly used filters are the

Sobel filter, the Laplacian operator, the difference of Gaussians, the Mexican hat, the Canny and so forth [2].



fig.1 Example original image[3]



fig.2. Example edge enhanced image[3]

In this paper, we describe an algorithm designed to enhance the edges after the pixel size is doubled linearly through an interpolation and to maintain the spatial resolution after the edge enhancement. Our algorithm is developed during the course of developing an X-ray

imaging system [4] based on a set of GEM plates [5]. The gas detectors are used to produce more electrons when compared with the solid photo-converters such as the micro-channel plates [6,7] but there are greater limitations in the spatial resolution when the gases are used. We describe in this paper the results of a study based on the EGS4 calculations for the spatial resolution of the gas detectors. The term ‘spatial resolution’ is used for the smallest width of a pair of aluminum strips that can be distinguished from each other when the gap between them is the same as the width of the strips. The thickness of the aluminum plate is fixed at 1cm for the Ar gas and 2cm for the lead plate for testing the Xe gas. The gas detector is assumed to be located directly below the aluminum strips when the images are generated.

2. EFFECTS OF THE DIFFERENT INPUT FUZZY SETS

In this section, we describe how the interpolated function will change as the different fuzzy sets are used as the input fuzzy sets in representing the functions of the form $z = f(x, y)$. Note that a gray scale image can be considered as a discretization of such a function. Given a gray scale image $\{a_{ij} | i=1,2,\dots,N, j=1,2,\dots,M\}$, we consider a fuzzy system $F(x, y) = \sum_{i,j=1}^{N,M} a_{ij} B_{ij}(x, y)$ where $B_{ij}(x, y)$'s are input fuzzy sets. We would like to see what difference there will be in the value of $F(x, y)$ when (x, y) is a non-grid point.

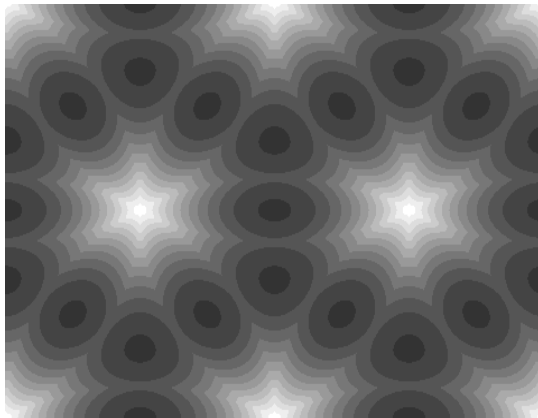


fig.3. Relative intensities by the cone shaped fuzzy sets

First, we examine the case where the cone is used as the input fuzzy sets. The fuzzy sets are centered at the 14 points; $(-1, 2\sqrt{3})$, $(1, 2\sqrt{3})$, $(-2, \sqrt{3})$, $(0, \sqrt{3})$, $(2, \sqrt{3})$, $(-3, 0)$, $(-1, 0)$, $(1, 0)$, $(3, 0)$, plus the four reflective points with respect to the x-axis, where the base radius of the cone is 2. For simplicity, we took the height of the cones at the center point is 1. We evaluated the membership values at the pixel points 480×320 . The minimum of the membership values is 1.0 and the maximum is found to be 1.26795. The relative intensity of the membership values of the points in the interval $[-2, 2] \times [-2, 2]$ is shown in fig.3. The four brighter spots are the points with the minimum value, while the surrounding darkest points are the pixels where the membership values take the maximum.

For the second example, we consider the two-dimensional radial basis function $f(r) = e^{-(r/\sigma)^2}$. We used 13×13 fuzzy sets centered at $x_i = -3 \pm 0.5i$, $i = 0, 1, 2, \dots, 12$ and $y_j = -3 \pm 0.5j$, $j = 0, 1, 2, \dots, 12$. At the 480×320 grid points of $[-2, 2] \times [-2, 2]$, we evaluated the membership values of the 169 fuzzy sets and added the results to obtain the relative intensity shown in fig.4. When $\sigma = 0.5$ is used, the maximum is found to be 3.14224 and the minimum is found to be 3.14093.

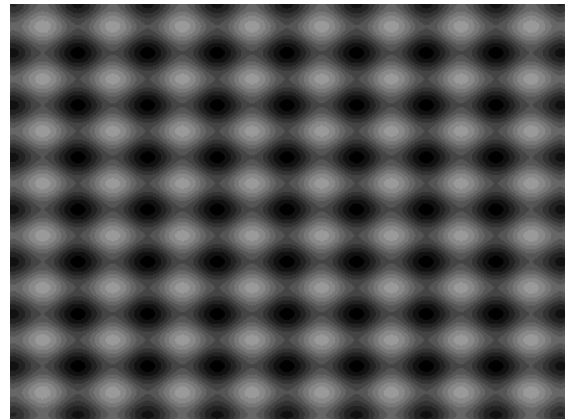


fig.4. Relative intensities by the radial basis functions

As the third example, we examined the cubic spline function in a polar form. We used the nine functions centered at $(1, 1)$, $(0, 1)$, $(1, 1)$, $(-1, 0)$, $(0, 0)$, $(1, 0)$, $(-1, -1)$, $(0, -1)$, $(1, -1)$ and evaluated them at the 480×320 pixel points in the interval $[-1, 1] \times [-1, 1]$. The maximum membership value is found to be 1.171573 and the

minimum is 0.965055. The relative intensities at the grid points are shown in fig.5.

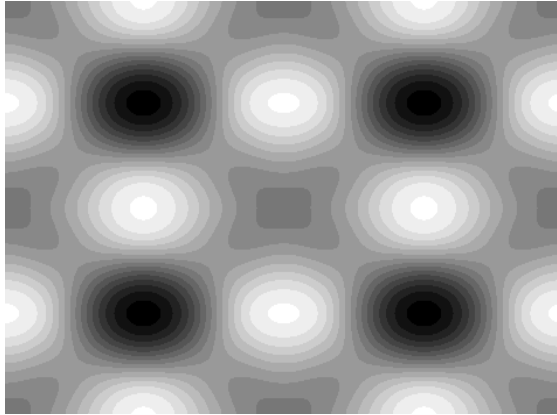


fig.5. Relative intensities by the rotated cubic spline

Finally, we checked the fuzzy sets obtained by taking the Cartesian product of two fuzzy sets such as $T_i(x) \times T_j(y)$ where $T_i(x)$, $T_j(y)$ are the triangular fuzzy sets and $B_i(x) \times B_j(y)$ where $B_i(x)$, $B_j(y)$ are the triangular fuzzy sets. The results show that they produce functions with a constant intensity at all the interpolated points. This can actually be proved analytically. Thus, we conclude that the Cartesian products of the 1-D fuzzy sets generate better interpolated values when compared with the other 2-D fuzzy sets.

3. EXAMPLE IMAGES GENERATED BY THE GAS DETECTORS

In this section, we consider the example images generated by the photons input to the object. The relative intensity is taken from the number of electrons generated and is obtained from the EGS4 calculations. The geometry used in the simulation for creating the images is shown in fig.6, where the object at the top is either an aluminum plate or a lead plate with three strips cut out and a gas layer is located below them with a vacuum layer in between. We counted the number of electrons generated inside the gas by putting artificial grids below the gas layer.

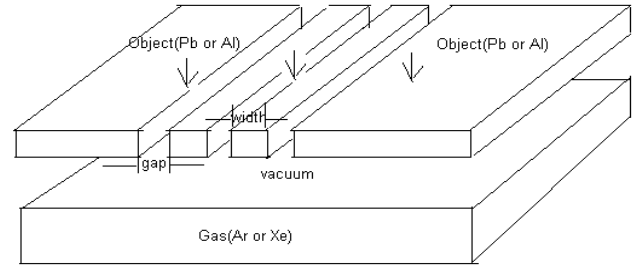
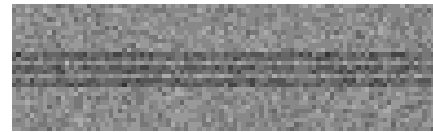
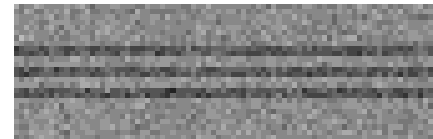


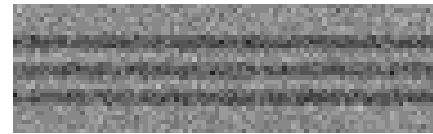
Fig.6. Geometry of the object for the image generation



Width-0.15mm, Gap-0.15mm



Width-0.2, Gap-0.2mm



Width-0.3mm, Gap-0.3mm

fig.7. Sample images generated by EGS4 for the Ar gas layer of 3mm thick



Width-0.15mm, Gap-0.15mm



Width-0.30mm, Gap-0.30mm



Width-0.40mm, Gap-0.40mm

fig.8. Sample images generated by EGS4 for the Xe gas layer of 0.5mm thick

All of the images in fig.7 and fig.8 were generated by EGS4 using 60keV X-rays. The X-ray source is located at a 50cm distance straight up from the center of the object and the distance from the object to the gas layer in fig.6 is 1mm. The images in fig.7 were generated when the aluminum of a thickness of 1cm is used with 9×10^9 photons input to the object in the 4π angle and the Ar gas is used. The images in fig.8 were generated when the lead (Pb) of a 2cm thickness is used as the object with 2×10^8 photons input to the object while Xe is used for the gas.

The dark strips indicate the taken out strips in between the aluminum (or lead) strips and the white areas are either the aluminum strip images or the aluminum plate images. The difference in the images of fig.7 and fig.8 comes from the difference in the electron ranges in the two different gases. Note that we used a lesser number of photons for the Xe gas than for the case of Ar gas. In the case when we use a lesser number of photons in fig.7, we would have images with the background whiter. However, the part of the images for the strips would become less clear.

By changing the number of photons input to the object, we generated different sets of images. We found that the noise in the parts of the strip objects cannot be removed by adjusting the number of photons. This noise comes essentially from the movement of the particles inside the gas. This is what makes the difference between the gas detectors and the solid detectors such as those using micro-channel plates. However, the gas detectors are preferred since the gases generate more electrons than the solid photo-converters even though the electrons have larger ranges in the gases.

4. EDGE ENHANCEMENT OF THE X-RAY IMAGE

In this section, we describe our algorithm designed to enhance the edges so that it maintains the spatial resolution and also increases the pixel size. Let the images shown in fig.7 and fig.8 be $P = \{p_{ij} \mid i, j = 1, 2, \dots, N\}$ with $p_{ij} \in \{0, 1, 2, \dots, 255\}$ where $N=100$. As a first step to increase the pixel size, we compute an approximate solution for the system of equations

$$\sum_{i,j=1}^N c_{ij} B_i(x_k) B_j(y_l) = p_{kl}$$

for $k, l = 1, 2, \dots, N$. Note that if we form an image using the coefficients c_{ij} after taking the integral parts and limit

them so that $0 \leq c_{ij} \leq 255$, then the image P can be considered as a smoothed image of $C = \{c_{ij} \mid i, j = 1, 2, \dots, N\}$.

To obtain a larger pixel size image, we interpolate the function $P(x, y) = \sum_{i,j} c_{ij} B_i(x) B_j(y)$. We use images of a size of 200 by 200. Note that we could have used p_{ij} instead of c_{ij} in the definition of the function $P(x, y)$. The resulting image, however, would be smoother than the original since the pixel values at the edges are smaller than the original.

Before we apply our edge enhancement algorithm to the images, we apply a 'noise' reducing algorithm to reduce the pixel values caused by the electrons which passed through the object. We simply apply a sigmoid type function of the form

$$\phi(x) = \frac{1}{1 + e^{-\alpha(x-x_0)}}$$

where x_0 is a threshold value and α is a scale factor. In the case where the pixel values x are normalized so that they are in the interval $[0, 1]$, then one can take α to be in the range of 10 to 30 and x_0 to be a number in the range of 0.3 to 0.75.

Next, we compute the gradient vector at each pixel of the resulting image. Assuming that $P(x, y)$ is the function obtained by the resulting image, i.e. c_{ij} replaced by the adjusted values c'_{ij} . One can either calculate the gradient directly from the cubic spline function or by calculating the convolution of the image with

$$\begin{pmatrix} (1,1) & (4,0) & (1,-1) \\ (0,4) & (0,0) & (0,-4) \\ (-1,1) & (-4,0) & (-1,-1) \end{pmatrix}.$$

At each pixel (k, l) , we compute the magnitude of the gradient and add it to the nearest neighboring pixel in the direction of the gradient. Note that we are not adding the magnitude of the gradient to the pixel value at (k, l) .

The left hand side image of fig.10 is an example image drawn from a constant multiple of the magnitude of the gradient at the corresponding pixel. The edges of the lead strips in fig.6 are shown in the figure. Note that the dark pixels are actually the neighboring pixels of the edges of the lead strips instead of the edge pixels themselves. The right hand side image of fig.10 is an image obtained by

shifting the constant multiple of the magnitude of the gradient to the nearest neighboring pixel in the direction of the gradient. One can see from this figure that there are some differences between the two images, e.g. the size of the gap between the two consecutive edge lines are different.

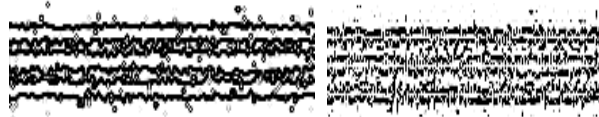


fig.10. Magnitude of the gradient (left) and the image after shifting(right)

Fig.11 shows a comparison of the image for the gradient and the image obtained by adding the shifted gradient. One can see from this figure that if the magnitude of the gradient on the left hand side is added directly to the original image, then the dark strips on the right hand side figure would become thicker and hence the spatial resolution of the resulting figure would get degraded.

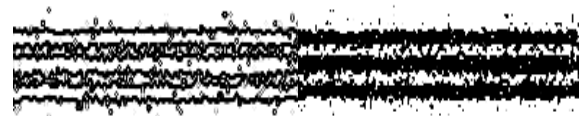
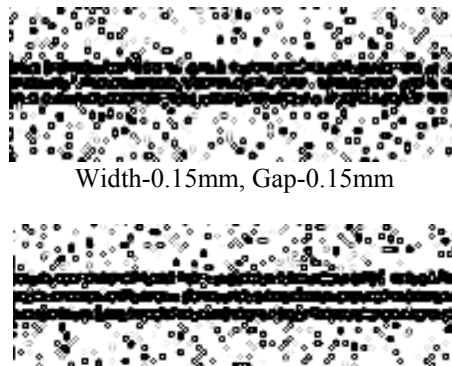


fig.11. Magnitude of the gradient (left) and the enhanced image (right)

Fig.12 shows the images generated from a constant multiple of the magnitude of the gradient computed from the three images in fig.7, i.e. the images of the aluminum strips generated by a 3mm thick Ar gas layer. The corresponding enhanced images generated by our algorithm are shown in fig.13. Note that the width of the dark strips and the width of the white strips look nearly the same. If we added the magnitudes of the gradient directly to the corresponding pixel values, the width of the black strips would have become larger.



Width-0.15mm, Gap-0.15mm



Width-0.20mm, Gap-0.20mm



Width-0.30mm, Gap-0.30mm

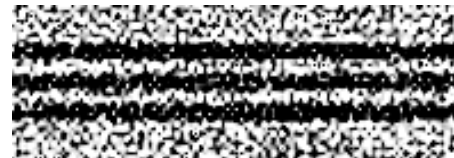
fig.12. Magnitude of the gradient for the images in fig.7 (Ar gas layer of 3mm thick)



Width-0.15mm, Gap-0.15mm



Width-0.20mm, Gap-0.20mm



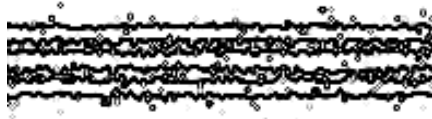
Width-0.30mm, Gap-0.30mm

fig.13. Enhanced images for the images of fig.7 (Ar gas layer of 3mm thick)

Fig.14 shows the images generated from a constant multiple of the magnitude of the gradient computed from the three images in fig.8, i.e. the images of the lead strips generated by a 0.5mm thick Xe gas layer. The corresponding enhanced images generated by our algorithm are shown in fig.15. Note here also that the width of the dark strips and the width of the white strips look nearly the same.



Width-0.15mm, Gap-0.15mm

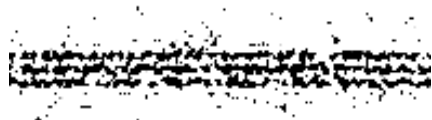


Width-0.30mm, Gap-0.30mm

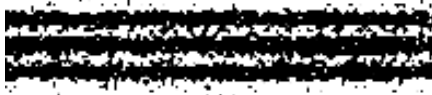


Width-0.40mm, Gap-0.40mm

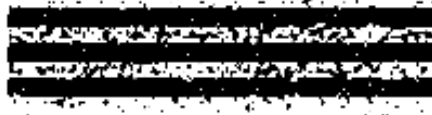
fig.14. Magnitude of the gradient for the images in fig.8
(Xe gas layer of 0.5mm thick)



Width-0.15mm, Gap-0.15mm



Width-0.30mm, Gap-0.30mm



Width-0.40mm, Gap-0.40mm

fig.15. Enhanced images for the images of fig.8
(Xe gas layer of 0.5mm thick)

5. CONCLUSION

We have shown that by adding the magnitude of the gradient at a pixel (k, l) to the pixel value of the neighboring pixel nearest to (k, l) in the direction of the gradient *enhances* the edge of the X-ray images. We have seen that this operation does not degrade the spatial resolution of the image. We have also shown that the pixel size can be increased through an interpolation using a cubic spline function. The spline function is an approximate representation of the image obtained by a very simple $O(N)$ operation for the images of a pixel size $N \times N$. Even though we have the edges enhanced without a degradation of the spatial resolution, the final images look rougher than the original. How to handle this problem is left for a future study.

Acknowledgements

This work has been carried out under the nuclear research and development program supported by the Ministry of Science and Technology of Korea.

REFERENCES

- [1] Medcyclopaedia, <http://www.amersham-health.com/>.
- [2] F. Cheevasuvit, K. Dejhan, A. Somboonkaew, Edge enhancement, using the transform of subtracted smoothing image, *Asian conference on Remote Sensing* (1992).
- [3] <http://www.inform.umd.edu/UMS+State/UMD-Projects/MCTP/Technology/image/>.
- [4] B.S. Moon, et al., *Development of a Gas Electron Multiplier Detector for a Digital Radiographic System*, KAERI/RR-2183/2001, Korea Atomic Energy Research Institute, 2001.
- [5] F.Sauli, *Nucl. Inst. Meth.*, A386, 531(1997)
- [6] R. K. Martin, J. H. Chappell and S. S. Murray, Relative Quantum Efficiency Measurements of CsI, CsBr and CsI/CsBr Coated Micro Channel Plates, *SPIE* Vol. 1344 (1990) 340-345.
- [7] G.A. Burginyon, B.A. Jacoby, J.K. Wobster, R.D. Ernst, D.S. Ancheta, K.G. Tirsell, Absolute detection efficiency of a micro-channel plate detector to X-rays in the 1-100 keV energy range, *SPIE* Vol. 1736 (1992) 36-42.